

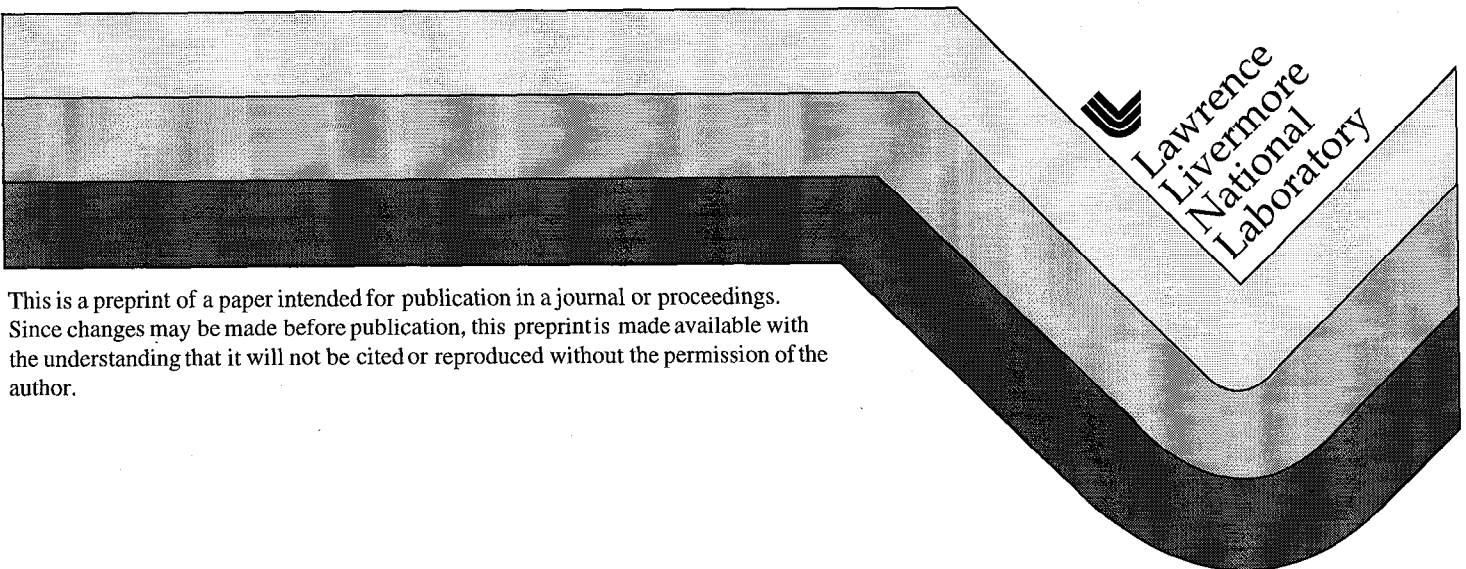
UCRL-JC-132568  
PREPRINT

# Macroscopic Magnetic Islands and Plasma Energy Transport

F. Porcelli  
E. Rossi  
G. Cima  
A. Wootton

This paper was prepared for submittal to the  
Workshop on Fusion Related Physics and  
Engineering in Small Devices  
Trieste, Italy  
October 6-8, 1998

December 3, 1998



This is a preprint of a paper intended for publication in a journal or proceedings.  
Since changes may be made before publication, this preprint is made available with  
the understanding that it will not be cited or reproduced without the permission of the  
author.

#### DISCLAIMER

This document was prepared as an account of work sponsored by an agency of the United States Government. Neither the United States Government nor the University of California nor any of their employees, makes any warranty, express or implied, or assumes any legal liability or responsibility for the accuracy, completeness, or usefulness of any information, apparatus, product, or process disclosed, or represents that its use would not infringe privately owned rights. Reference herein to any specific commercial product, process, or service by trade name, trademark, manufacturer, or otherwise, does not necessarily constitute or imply its endorsement, recommendation, or favoring by the United States Government or the University of California. The views and opinions of authors expressed herein do not necessarily state or reflect those of the United States Government or the University of California, and shall not be used for advertising or product endorsement purposes.

# Macroscopic magnetic islands and plasma energy transport

F. Porcelli<sup>1</sup>, E. Rossi<sup>1</sup>, G. Cima<sup>2</sup>, A. Wootton<sup>3</sup>, LLNL

*Istituto Nazionale Fisica della Materia, Department of Energetics,  
Politecnico di Torino, Italy, <sup>2</sup>Fusion Research Center, University of Texas at  
Austin, U.S.A.*

*<sup>3</sup>Lawrence Livermore National Laboratory*

## ABSTRACT

A model is presented, based on the combined effects of  $m=n=1$  magnetic island dynamics, localized heat sources, large heat diffusivity along magnetic field lines and plasma rotation, which may explain the multip peaked temperature profiles and transport barriers observed in tokamak plasmas heated by electron cyclotron resonant waves.

Experiments in magnetically confined, high temperature plasmas heated by intense electromagnetic waves at the electron cyclotron resonance frequency, have revealed peculiar and hitherto unexplained plasma behavior. The most striking results [1], come from the Rijnhuizen Tokamak Project (RTP) where electron cyclotron heating (ECH) with maximum power  $P \approx 360\text{k W}$  is applied to the toroidal plasma. In this experiment, a double-pulse, multiposition Thomson scattering diagnostic measures the electron temperature profile with a very high spatial resolution. In the plasma central region, led the TRP group to suggest a "filamentary" structure. In addition ECH experiments in TRP [2] have revealed very sharp temperature gradients just outside the sawtooth mixing radius. Other minor structures in the  $T_e$  profiles are sometimes observed near rational surfaces with  $q > 1$ . The sharp gradients at the sawtooth mixing radius, as well as the other minor structures, have been interpreted as due to the presence of "transport barriers" on rational  $q$  surfaces +[1]-[3].

The RTP results have raised the question whether the observed peculiar behavior is specific to ECH, or whether it is in fact universal to all tokamak plasmas, but can be recognized only with a sophisticated temperature diagnostics. Clearly, an answer to this question relies on our understanding of the underlying magnetic structure. It must be emphasized that this structure in the plasma central region is strongly affected by the so-called sawtooth relaxation oscillations [4], associated with the instability of a resistive kink mode with toroidal  $n=1$  and dominant poloidal  $m=1$  mode numbers, which results in a periodically growing  $n=m=1$  magnetic island.

Peculiarities in plasma behavior in the presence of ECH have been reported in other tokamaks as well. In this Letter, we shall concentrate on results from the Texas Experimental Tokamak Upgrade (TEXT-U) [5]. These results, together with nonstandard sawtooth traces observed in other ECH tokamak experiments (see, e.g., Ref. [6] and other references therein), strongly suggest that the peculiar behavior is the outcome of an interplay between sawteeth and ECH. The objective of this Letter is to clarify this interplay from a theoretical standpoint. We present a model for the evolution of the electron temperature profiles, based on the following essential ingredients: (i) a reconstruction of magnetic surfaces based on the sawtooth reconnection process; (ii) the presence of a localized electron heat source; (iii) the effect of plasma rotation; (iv) the effect of anisotropic heat diffusion, whereby the parallel (along the field lines) heat diffusion coefficient,  $\chi_{\parallel}$ , is taken as very large, and the perpendicular coefficient,  $\chi_{\perp}$ , as relatively small, on the sawtooth period time scale and spatial extent. This model is able to reproduce qualitatively the observed features of the TEXT-U and RTP temperature profiles, in particular sharp gradients at the sawtooth mixing radius and several peaks, even when a strictly constant  $\chi_{\perp}$  profile is assumed. What is special with ECH, in contrast with other heating schemes, is that electron cyclotron waves transfer their energy directly to the electrons, with no delay and in a very localized deposition region [7]. This heat is then transported very rapidly along field lines to electrons in other parts of the plasma because of very large parallel heat conduction and plasma rotation. These features are fully exploited in our model.

Let us first summarize the relevant results from TEXT-U, [5]. The main tokamak parameters are  $R=1.05\text{m}$ ,  $a=0.27\text{m}$ ,  $B \approx 2\text{T}$ ,  $I_p \approx 230\text{kA}$  and central electron density  $n_e \approx 3.0 \times 10^{19}\text{m}^{-3}$ . The experiment is equipped with an ECH system which delivers a maximum power  $P \approx 270\text{kW}$ . The electron

temperature is measured by an Electron Cyclotron Emission (ECE) diagnostic. The typical spatial resolution of the ECE signal is  $O(1\text{cm})$ , which is not as good as the Thompson scattering system on RTP. On the other hand, the ECE diagnostic on TEXT-U has a very high temporal resolution,  $O(20\mu)$ , over an extended time interval. In this sense, the temperature measurements on TEXT-U can be considered as complementary to those on RTP.

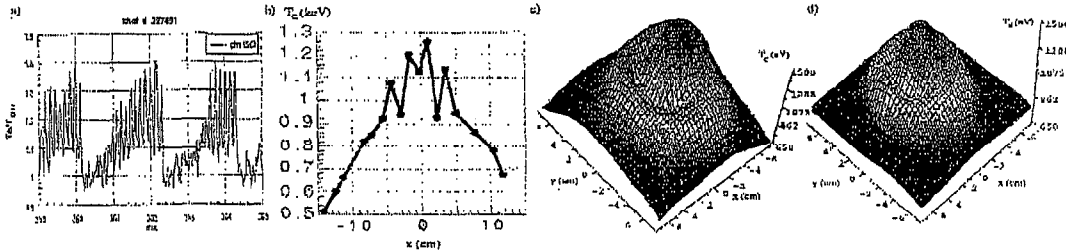


Figure 1: Electron temperature in TEXT-U. (a): central  $T_e$  evolution; (b): an example of  $T_e$  profiles; (c) and (d): 3-D reconstructions.

Figure 1 shows an example of the central electron temperature evolution in TEXT-U. Shown in figure 1(a) are nearly three sawtooth ramps, with a period  $\tau_{saw} \approx 2\text{ms}$ , and with fast oscillations superimposed. The period of the fast oscillations matches the plasma toroidal rotation period,  $\tau_{rot} \approx 160\mu$  in this case. If these oscillations are indeed due to the presence of an  $m=1$ ,  $n=1$  magnetic island, then this island is formed early on during each sawtooth ramp and maintains a nearly saturated amplitude for most of the ramp. These ramps look different from Ohmic sawtooth ramps in TEXT-U, which exhibit detectable MHD fluctuations only near the tops. This suggests that the auxiliary heating influences  $m=n=1$  mode stability, perhaps indirectly through the production of peaked pressure profiles. Fig. 1(b) presents an example of an ECE  $T_e$  profile; a sequence of these profiles can be found in Fig. 10 of Ref. [5]. The profiles at time intervals  $t_2 - t_1 \approx \tau_{rot}$  nearly coincide, which confirms that we are indeed observing a toroidal  $n=1$  structure. These profiles exhibit four to five peaks and are similar to the filament-like temperature structures previously reported in RTP. However, the RTP observations lack time history. With the temporal and spatial resolution available on TEXT-U, we find that the structures are cyclic and consistent with a fixed structure in the rotating plasma frame. The main poloidal  $m=1$  structure

can be deduced from 3-D reconstructions of the type shown in Figs. 1(c),(d), where the time variable has been transformed into the poloidal angle variable under the assumption of rigid rotation.

Let us now present our theoretical model. We assume, for simplicity, a "rectified" tokamak, i.e. a cylindrical plasma column with periodic boundary conditions at the cylinder bases ( $z=0$  and  $z=L$ ). In the absence of an  $m=1$  island, magnetic surface cross sections are concentric circles of constant normalized helical flux,  $\psi_{*in}(r) = \int_0^{r^2} [q_{in}(z)^{-1} - 1] dz$ , where the subscript "in" stands for "initial", i.e. before the island formation. For a typical (i.e. monotonic)  $q_{in}(r)$  profile,  $\psi_{*in}(r)$  has a maximum at the  $q_{in} = 1$  radius,  $r = r_s$ . The growth of an  $m=1$  island is brought about by a rigid shift of surfaces within the original  $q_{in} = 1$  surface. The helical flux,  $\psi_*(r, \alpha; t)$ , where  $\alpha = \theta - 2\pi z/L$ , remains nearly constant on moving fluid elements. At each stage of the reconnection process, the island separatrix is formed by two circles of radii  $r_{1sp} < r_s$  and  $r_{2sp} > r_s$ , where  $\psi_{*in}(r_{1sp}) = \psi_{*in}(r_{2sp})$ , with the center of the inner circle (i.e. the original magnetic axis) displaced from its initial position by a distance  $\xi(t) = r_{2sp} - r_{1sp}$ . In addition, toroidal flux conservation is assumed; with  $B_z \approx const$ , this is equivalent to area conservation, i.e. when the island separatrix later evolves into the croissant-shaped surface, the area encircled in the poloidal plane by the surface is constant and equal to  $A = \pi(r_{2sp}^2 - r_{1sp}^2)$ . The contour of the croissant is also a surface of constant helical flux, specifically  $\psi_*(r, \alpha; \xi) = \psi_{*in}(r_{1sp})$ . This model for the  $m=n=1$  island evolution is based on the specific convection pattern associated with the  $m=n=1$  resistive internal kink mode [8] and on the ideal MHD assumption of frozen magnetic flux through moving fluid elements, approximately valid everywhere except in the immediate neighborhood of the island X-point and current sheet.

The well known Kadomtsev model [9] for the sawtooth relaxation corresponds to the two basic reconnection rules described above and to the following assertions: (i) the reconnection process proceeds until full reconnection, i.e. until  $\xi(t)$  attains its maximum value,  $r_{mix}$ , called mixing radius and defined by  $\psi_{*in}(r_{mix}) = \psi_{*in}(0)$ ; when  $\xi = r_{mix}$ , poloidal symmetry is restored, the island O-point having evolved into the new magnetic axis, while the island X-point and the original axis annihilate each other; (ii) the time for  $\xi$  to evolve from  $\xi \approx 0$  to  $\xi = r_{mix}$  is  $\tau_K \approx (\tau_R \tau_A)^{1/2}$ , with  $\tau_A$  a typical Alfvén time and  $\tau_R$  the global resistive diffusion time. In our model, we assume that the island growth initially follows the two basic rules of the helical

flux and area conservation, but does not necessarily evolve to full reconnection. In addition, we do not attempt to describe the dynamical evolution; rather, the function  $\xi(t)$  is inferred from the experiments. We observe, however, that  $\tau_K = O(1\text{ms})$  for TEXT-U parameters, in fair agreement with the experimental sawtooth period.

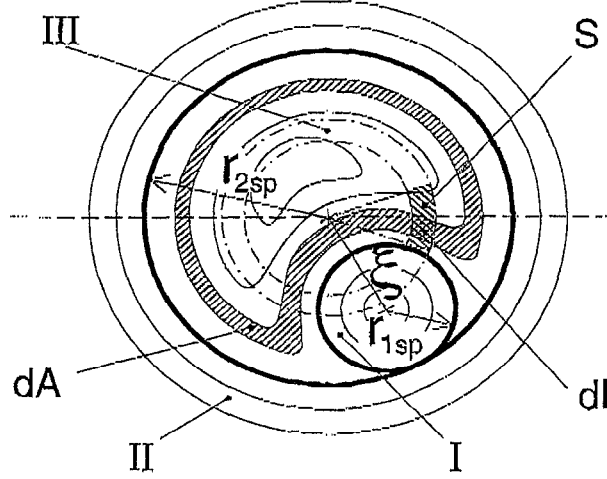


Figure 2: Magnetic island topology;  $S$  is the heat source.

Our problem, now, is to specify a function  $\psi_*(r, \alpha; t)$  whose contour levels correspond to croissant-shaped surfaces of the type shown in region III of Fig. 2, satisfying the basic reconnection rules. These rules do not define a unique solution for the functional  $\psi_*$ , although they represent a rather strong mathematical constraint. We find it convenient to introduce a Hamiltonian for the magnetic field lines inside the island separatrix (region III of),  $H = H(\psi_*) = H(r, \alpha; \xi)$ , such that

$$H = \frac{(r^2 + \xi^2 - 2\xi r \cos \alpha - r_{1sp}^2)(r_{2sp}^2 - r^2)}{r^2 + \xi^2 - 2\xi r \cos \alpha} \quad (1)$$

with  $\psi_{*in}(r)$  and  $\xi(t)$  prescribed functions. The island separatrix for a given  $\xi$  corresponds to the contour level  $H = 0$ , while  $H$  reaches a maximum

value,  $H_{max}(\xi)$ , on the island O-point. Croissant-shaped magnetic surfaces correspond to contour levels  $H = H_0 \in [0, H_{max}]$ . Note that the curves  $H(r, \alpha; \xi) = H_0$  become circles in both limits  $\xi = 0$  and  $\xi = r_{mix}$  (in the latter limit,  $r_{1sp} = 0$ ). The function  $H = H(A)$  can be evaluated numerically after computing the area,  $A$ , pertaining to each  $H = H_0$  surface; from this, the area conservation rule, the function  $H = H(\psi_*)$  can be easily constructed. Outside the island separatrix (regions I and II of Fig. 2) the magnetic surface cross-sections are circular.

Also represented in Fig. 2 is an electron heat source,  $S$ , localized on the poloidal midplane between radii  $r_{h1}$ ,  $r_{h2}$  and angles  $\theta_{h1}$ ,  $\theta_{h2}$ . Since parallel heat conduction is very large, the deposited heat spreads rapidly and uniformly over all flux tubes intersecting the heat deposition region. Then, taking into account plasma rotation (assumed to be rigid for the sake of simplicity), the heated region as seen in the plasma rest frame rotates with angular frequency  $\omega_{rot}$ . Thus, in the plasma frame for  $S = S(r, \theta, t)$  we have  $S = \rho [\mathcal{H}(r - r_{h1})(r_{h2} - r)] \cdot [\mathcal{H}(\omega_{rot}t - \theta_{h1})(\theta_{h2} - \omega_{rot}t)]$  where  $\mathcal{H}$  is the Heavyside function,  $\rho = P/V_h$  and  $V_h$  is the deposition volume. Now, if we denote by  $dA$  the cross-sectional area at a generic flux tube and by  $dI$  its intersection with the heated region (Fig. 2), we can write the ECH power density averaged over flux surfaces as  $\langle S \rangle(A) = \rho dI/dA$ . Note that the heat is transported radially by parallel heat diffusion in a complex magnetic structure such as that of Fig. 2, resulting in an apparently nonlocal heat transport process.

Let us now discuss how the plasma density and pressure evolve during the growth of the  $m=n=1$  island. Let us disregard, for a moment, the heat source and perpendicular diffusion process. In addition, we neglect magnetic to thermal energy transfer; we have checked that this accounts for only about 1 ÷ 2% of the transferred heat. Then the area conservation rule implies the following conservation law for the plasma pressure,  $\pi \int_{r_{1sp}}^{r_{2sp}} p(r^2) dr^2 = \int_A p(A') dA'$ , which in differential form becomes

$$p(A) = \pi \left[ p(r_{2sp}^2) \frac{dr_{2sp}^2}{dA} - p(r_{1sp}^2) \frac{dr_{1sp}^2}{dA} \right] = p(\psi_*) \quad (2)$$

since  $A = A(\psi_*)$  through Eq. (1). The plasma density obeys completely similar relations. We make the simplifying (and experimentally verified [1], [5]) assumption of a flat electron density. Then, since  $p = nT$ , Eq. (2) can be written for the temperature as well.

If we now consider the presence of the heat source and the effect of perpendicular heat diffusion, then the pressure and the temperature will depend explicitly on time:  $T = T(A, t)$ . In this Letter, we assume  $\chi_{\perp} = \text{const}$ . It is convenient to specify the heat transport equation in a Lagrangian frame of reference. We also have to take into account the different topology of the three regions I,II,III. Thus, in region III, we obtain the diffusion equation

$$\frac{3}{2} \frac{\partial T}{\partial t} = \chi_{\perp} \left( \langle |\nabla A|^2 \rangle \frac{\partial^2 T}{\partial A^2} + \langle \nabla^2 A \rangle \frac{\partial T}{\partial A} \right) + \frac{\langle S \rangle}{n}; \quad (3)$$

Similar equations apply to regions I and II, with  $A = \pi r^2$  and  $r$  indicating the distance from the displaced axis in region I. The time evolution of the three regions is specified by the displacement function  $\xi(t)$  and by  $\psi_{*in}(r)$ , together with Eq. (1). The solution of Eq.(3) requires an initial condition,  $T(r, t = 0) = T_{in}(r)$ , where at  $t = 0$ ,  $\xi(0) = 0$ , and the following boundary conditions: a condition at the edge of the integration domain,  $\bar{r} \approx 1.5r_{mix}$ , located in region II, specifically  $T(\bar{r}, t) = T_{in}(\bar{r})$ ; the geometrical conditions  $(\partial T_I / \partial r_1)_{r_1=0} = (\partial T_{III} / \partial A)_{A=0} = 0$  on the two magnetic axes of regions I and III, respectively. Finally, a condition on the separatrix is required. Note that, with  $\chi_{\perp} = 0$ , a discontinuity of the temperature across the separatrix is in general allowed by (2). With finite  $\chi_{\perp}$ , a common temperature is achieved approaching the separatrix from any of the three regions I,II,III, which is determined by the continuity of the heat flux. Equations (1-3), with the appropriate initial conditions as described above, completely specify our simulation model.

We present a typical solution obtained for the following input parameters [5]: (i) initial helical function  $\psi_{*in}(x) = (\Delta q / q_0) r_{mix}^2 x^2 (1 - x^2)$ , where  $\Delta q = 1 - q_0 = 1/16$ , and  $x \equiv r / r_{mix}$ ; (ii) a specified displacement function,  $\xi(t)$ , inferred from experimental data and shown in Fig.3(a); (iii) a power source  $P = 180\text{kW}$ ,  $w_{h1} = 0.3$  and  $w_{h2} = 0.4$ ; (iv) a sawtooth period  $\tau_{saw} = 2\text{ms}$ ; (v) a value  $\chi_{\perp} = 0.05\text{m}^2/\text{s}$ , (vi) a normalized rotation period,  $\tau_{rot} / \tau_{saw} = 1/18$ ; (viii) an initial temperature profile,  $T_{in}(r) = T_0(1 - r^2/a^2)$ , with  $T_0 = 0.8\text{keV}$ . Tridimensional reconstructions of the simulated electron temperature at various phases during the growth of the  $m=n=1$  magnetic island are shown in Figs. fig3(b),(c). Shown in Figs. 3(d)-(f) are examples of the simulated temperature profiles. These figures should be compared with the TEXT-U measurements in Fig.1 (see also Figs 10,11 of Ref [5]), as well as the RTP temperature profiles in Figs. 3-4 of [1]. The similarities are quite

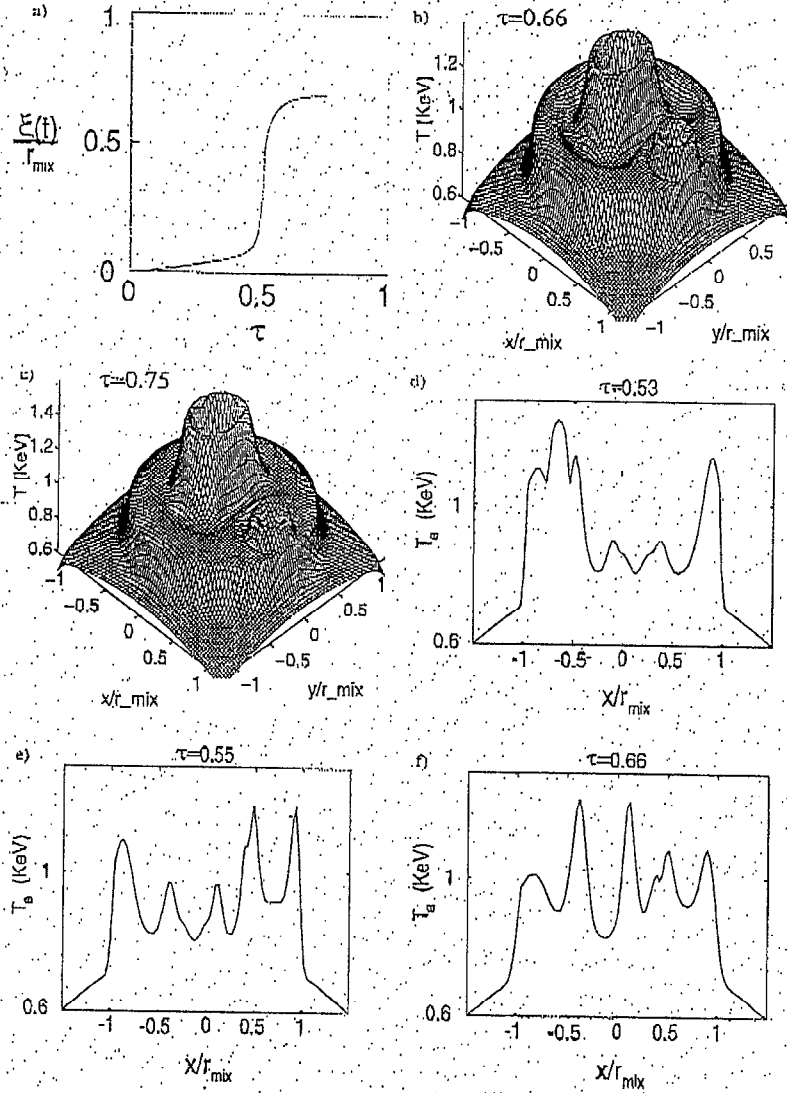


Figure 3: Simulation results. (a): displacement function,  $\tau \equiv (t - t_0)/\tau_{saw}$ ; (b),(c): examples of 3-D reconstructions of  $T_e$ ; (d),(e),(f): examples of  $T_e$  profiles.

evident. In particular, our model is able to reproduce temperature profiles with four to five peaks, fairly independently of the precise size and localization of the heat absorption region. In principle, more peaks are possible with more structured displacement function,  $\xi(t)$ . In addition, our model predicts the formation of sharp temperature gradients just outside the mixing radius. This is clear from the 3-D plots in Figs. 3(c,d), where the outer, circular, rim structure corresponds to a region centered on the plot of the island separatrix bordering region II. The rim structure is also quite evident from the TEXT-U experiment reconstructions shown in Figs. 1(c,d).

We stress that the multi-peaked structure and the sharp gradients are obtained in the simulation even with a constant  $\chi_{\perp}$ . Indeed, the sharp gradients are a result of heat convection, rather than diffusion. They are formed as the specific  $m=n=1$  resistive internal kink convection pattern advects the heat deposited inside the  $q = 1$  radius to the separatrix region at a rate faster than the heat diffusion rate.

We can think of two possible directions for the refinement of the present model. First, one may consider a temperature-dependent diffusion coefficient. If  $\chi_{\perp}$  were lower where the temperature is higher, the peaks in the electron temperature profile would become even sharper. Secondly, one may relax the single helicity assumption for the island evolution. For instance, the  $m=2$ ,  $n=1$  satellite harmonic for the helical flux perturbation would create a band of stochasticity in the field structure centered around the separatrix [10]. Clearly, a fully stochastic magnetic field would not support temperature gradients. All we can say, at the moment, is that judging from the experimental data, this band of stochastic field lines should be relatively narrow during most of the sawtooth ramp.

In conclusion, we have presented a theoretical model that is able to explain the observed multi-peaked temperature profiles, previously referred to as temperature filamentation [1], in ECH experiments. In addition, the model predicts the formation of sharp gradients near the sawtooth mixing radius. The model is based on the combined effects of  $m=n=1$  island dynamics, localized heat source, very large heat diffusivity along magnetic field lines and plasma rotation. The "transport barrier" just outside the sawtooth mixing radius is in fact a consequence of  $m=n=1$  heat convection, rather than reduced perpendicular heat diffusion near the  $q = 1$  rational surface. We may expect that the sometimes observed minor structures in the electron temperature profile at rational  $q$  values can be explained along similar lines, i.e. as

a consequence of macroscopic island dynamics with  $m/n = q_{\text{rational}}$ .

The authors wish to acknowledge useful discussion with Drs. N.J. Lopez Cardozo, A. Pöchelon and A. Pyrzyk. One of us (F.P.) was supported in part by the Italian Research Council (C.N.R.), while A.W. acknowledges the Texas Atomic Energy Research Foundation for financial support.

## References

- [1] N. J. Lopez Cardozo *et al.*, Phys. Rev. Lett., **73**, 256, (1994).
- [2] M. R. de Baar *et al.*, Phys. Rev. Lett., **78**, 4573, (1997).
- [3] N. J. Lopez Cardozo *et al.*, Plasma Phys. Contr. Fusion, **39**, B303, (1997).
- [4] von Goeler *et al.*, Phys. Rev. Lett., **33**, 1201, (1973).
- [5] G. Cima *et al.*, Plasma Phys. Contr. Fusion, **40**, 1149, (1998).
- [6] Z. A. Pietrzyk *et al.*, submitted to Nucl. Fusion, (1998).
- [7] V. Erckmann and U. Gasparino, Plasma Phys. Contr. Fusion, **36**, 1869, (1998).
- [8] B. Coppi *et al.*, Fiz. Plasmy, **2**, 961, (1976); [Sov. J. Plasma Phys., **2**, 533, (1976)].
- [9] B. B. Kadomtsev, Fiz. Plasmy, **1**, 710, (1975); [Sov. J. Plasma Phys., **1**, 389, (1975)].
- [10] A. J. Lichtenberg, Nucl. Fusion, **24**, 1277, (1984).

This work was performed under the auspices of the U.S. DOE by LLNL under contract No. W-7405-Eng-48.